



Assessing, surface morphology, optical, and electrical performance of ZnO thin film using ALD technique

S.S. Fouad · M. Nabil · B. Parditka · A.M. Ismail ·
E. Baradács · H.E. Atyia · Zoltán Erdélyi

Received: 30 March 2023 / Accepted: 23 July 2023
© The Author(s), under exclusive licence to Springer Nature B.V. 2023

Abstract In this study, we focus on the influence of the deposition process of ZnO thin films with a thickness of 250 nm—grown on glass and silicon substrates by atomic layer deposition (ALD) technique—on morphology, optical properties, AC conductivity, and dielectric properties. The atomic structure of the ZnO film was analyzed using scanning electron microscopy (SEM), energy dispersive X-ray spectrometer (EDX), and incident X-ray diffraction pattern (XRD). The XRD pattern confirms the presence of a crystalline phase, which is clearly observed in the SEM image. The crystallite size value was found to be

equal to 35.41 nm. Transparency study was performed by UV-vis spectroscopy. A key element of this study was to prove that it is impossible to attribute the optical energy gap (E_g) and refractive index (n) dependence to any typical thin film material because these parameters depend on the deposition condition and growth temperature. The values of the optical energy gap and the refractive index estimated from the absorption spectrum ($E_g = 3.32\text{eV}$, $n = 2.29$) were compared with those obtained from the transmittance and reflectance measurements ($E_g = 3.36$, $n = 2.272$). A new relation has been proposed based on the best fit for calculating the refractive index, which has been determined and compared with the values estimated by different researchers, showing excellent agreement. Electrical parameters such as dielectric characteristics and AC conductivity were also estimated at different temperatures ranging from 303 to 413 K versus the frequency ranging from 1 kHz to 1 MHz. AC conductivity behavior was studied to explore the mechanism of conduction. Further analysis revealed that the correlated barrier hopping (CBH) model is the predominant theoretical model for elucidating the conduction mechanism existing in our ZnO thin film. This article contains recent advances in the modified ZnO metal oxide prepared by ALD, which is an efficient approach for sensor device fabrication, mainly depending on the estimated parameters.

S. Fouad · A. Ismail · H. Atyia
Department of Physics, Faculty of Education, Ain Shams
University, Cairo 11566, Egypt

M. Nabil (✉)
Department of Basic Engineering Sciences, Faculty
of Engineering (Shoubra), Benha University, Benha 13511,
Egypt
e-mail: mohammed_diab35@yahoo.com; mohamed.
mohamed04@feng.bu.edu.eg

B. Parditka · E. Baradács · Z. Erdélyi
Department of Solid-State Physics, Faculty of Science
and Technology, University of Debrecen, P.O. Box 400,
Debrecen 4002, Hungary

E. Baradács
Department of Environmental Physics, Faculty of Science
and Technology, University of Debrecen, Poroszlay u.6,
Debrecen 4026, Hungary

Keywords Atomic layer deposition mechanism · X-ray grazing · Dispersion parameters · Dielectric properties · AC conductivity · Thin layer · Sensor device relevance

Introduction

In recent years, knowledge of the optical band gap and the refractive index is vital to scrutinize the atomic structure, electronic band structure, and optical and electrical properties. The refractive index and the optical band gap are the most significant parameters to provide optical behavior [1–3]. Therefore, accurate measurements and calculation of optical parameters are essential.

The study of optical absorption provides essential information about the band structure and the energy gap in crystalline and non-crystalline materials, while the refractive index is an important parameter for the design of prisms, windows, and optical fibers, and for providing information about the chemical bonding and electronic structure as well. Zinc oxide thin films are of worldwide attraction due to their lower cost, optical, physical, chemical, and electronic properties, high refractive index, high chemical stability, and excellent transmittance of visible light, leading to a wide application in solar cells and in the field of industrial electronics, and many other areas of applications. Among the different thin film deposition methods, the RF magnetron sputtering is considered as one of the promising deposition method [4–12].

ZnO is a strong candidate for the channel layer in thin film transistors because ZnO material can be prepared at low temperatures with good electrical properties. The characteristics are strongly dependent on the structure and crystallinity of ZnO [13–17]. The direct band gap of ZnO with ≈ 3.37 eV at room temperature is attractive as a promising material for optoelectronic devices such as light-emitting diodes, solar cells, and transparent thin film transistors. Analysis of absorption spectra provides essential information on the band structure and the energy gap, while the refractive index provides information on the chemical bonding and electronic structure [18, 19].

In the present work, the ZnO thin film was prepared by atomic layer deposition (ALD) to produce high-quality films with a thickness of 250 nm. A precise comparative study of the preparation conditions

and their optical properties, including the optical energy gap and refractive index of ZnO thin films, deduced from the absorbance, transmission, and reflectance spectra, has been shown. In addition, the dielectric properties and AC conductivity were also studied and analyzed to provide additional insight into the mechanism that shows the outstanding properties of ZnO in devices, photocatalytic activities, and storage devices.

Experimental techniques

Material preparation

ZnO films have been prepared in a Beneq TFS-200 ALD system with a nominal thickness of 250 nm on glass and Si (100) at 203 °C in thermal mode in 1806 cycles. Two pieces of 2 by 2 cm and one piece of 0.5 by 0.5 cm glass and Si (100) substrates were placed in the middle of the reactor, respectively. The first reactant, in our case DEZ (diethylzinc from DOCK/CHEMICALS, transparent conductive oxide grade, TCO grade), is introduced into the ALD reactor chamber (DEZ pulse phase), which reacts with the substrate surface through self-limiting and saturating chemical reactions. Subsequently, the remaining chemical substances are removed (DEZ purge phase). The second reactant, in our case, deionized water (H₂O), is then introduced into the ALD reactor chamber (H₂O pulse phase), which also reacts with the surface in a self-limiting and saturating manner. The residual chemicals are then again extracted (H₂O purge phase). A schematic diagram of the ALD process for preparing the ZnO (250 nm) thin films can be seen in detail in Fig. 1(a). The pulse time and the purge time were 0.3 and 3 seconds, respectively, for both the DEZ and H₂O precursors. The parameters of MFC-NOP (mass flow controller for carrier gas and inert gas valving) and MFC-NOV (mass flow controller for vacuum chamber flow) of nitrogen gas inlets for ZnO were 300 and 300 sccm, respectively. The pressure in the main chamber stabilized at ~ 8 mbar while ~ 1 mbar in the reactor. To reduce the possibility of covering the backside of the glass samples, which could later affect the measurements, we fixed all four sides of the samples to the reactor plate with Kapton tape.

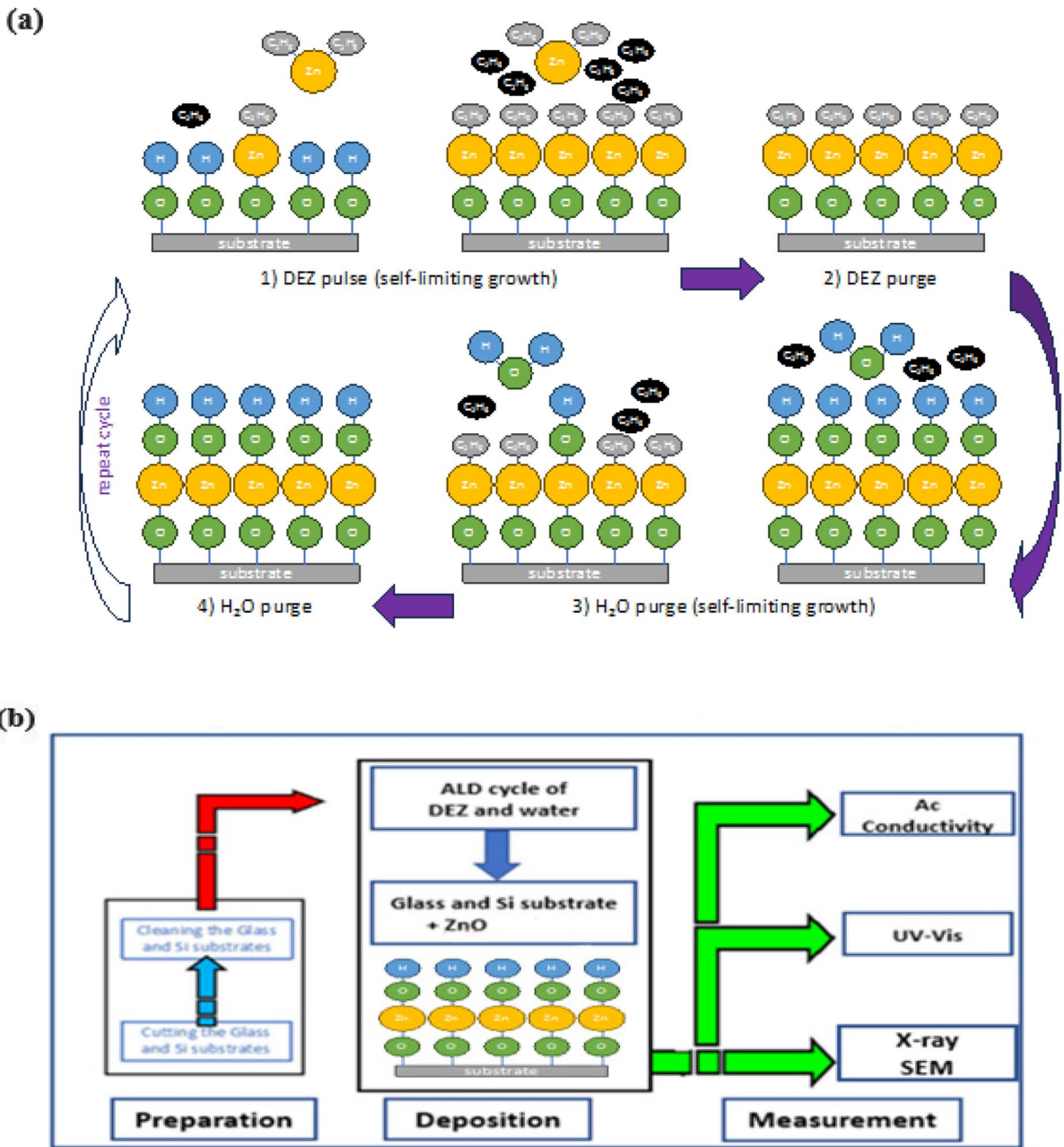


Fig. 1 a Schematic diagram of the ALD process for preparing the ZnO thin films and (b) flow chart of the experimental steps

Measurements

The thickness of the samples was measured by variable angle spectroscopic ellipsometry (Semi-lab SE-2000) and was found to be 250 nm. The microstructure and composition of the samples were determined by an energy-dispersive X-ray

spectrometer (EDX) connected to a field emission scanning electron microscope (FE-SEM) (QUANTA FEG 250 model). For the XRD analysis, we used a Rigaku Smart Lab 9 kW X-ray diffractometer. The measurements were performed in Bragg-Bretano () geometry with a rotating Cu anode (). The range of interest and the step size

were chosen to be 0 and 01°, respectively. The optical absorbance, transmittance, and reflection measurements were recorded using a double beam spectrophotometer (UV-3101PC Shimadzu in the wavelength range of 300–700 nm). The dielectric properties and AC conductivity of the investigated samples were measured using an automated RLC meter (FLUKE PM6306) in the frequency range (1 kHz to 1 MHz) and temperature range (303–413 K). The flowchart of the experimental steps can be seen in detail in Fig. 1(b).

Results and discussion

Structural modification

A high-resolution SEM was used to determine the surface morphology of ZnO (250 nm), as shown in Fig. 2(a).

The elemental mapping distribution of Zn and O is also presented in Fig. 2(b). Furthermore,

energy dispersive X-ray spectroscopy (EDX) was hired to examine the elemental ratio of the ZnO thin film as shown in Fig. 2(c). The analysis shows an insignificant variation in the composition of the as-prepared sample, confirms the presence of Zn and O elements in the ZnO film, and proves the stoichiometry of the prepared film. The XRD results of the ZnO thin films are shown in Fig. 3.

The XRD pattern reveals a crystalline structure with a wurtzite (hexagonal) phase and a preferred orientation 001 along the c-axis. Characteristic diffraction peaks were found at 31.5°, 34°, and 37° of the 2θ angle, respectively, corresponding to the hexagonal crystalline nature of ZnO thin films. The correlation between structural and optical properties suggests that the crystallite size of the films is predominantly influenced by the band gap. Furthermore, by plotting the normalized and fitted ZnO (100) peaks for the as-deposited sample, as seen in the inset of Fig. 3, we can obtain the approximate grain size by Scherrer's formula

Fig. 2 a SEM images, b elemental mapping, and c EDX spectra, for ZnO (250 nm)

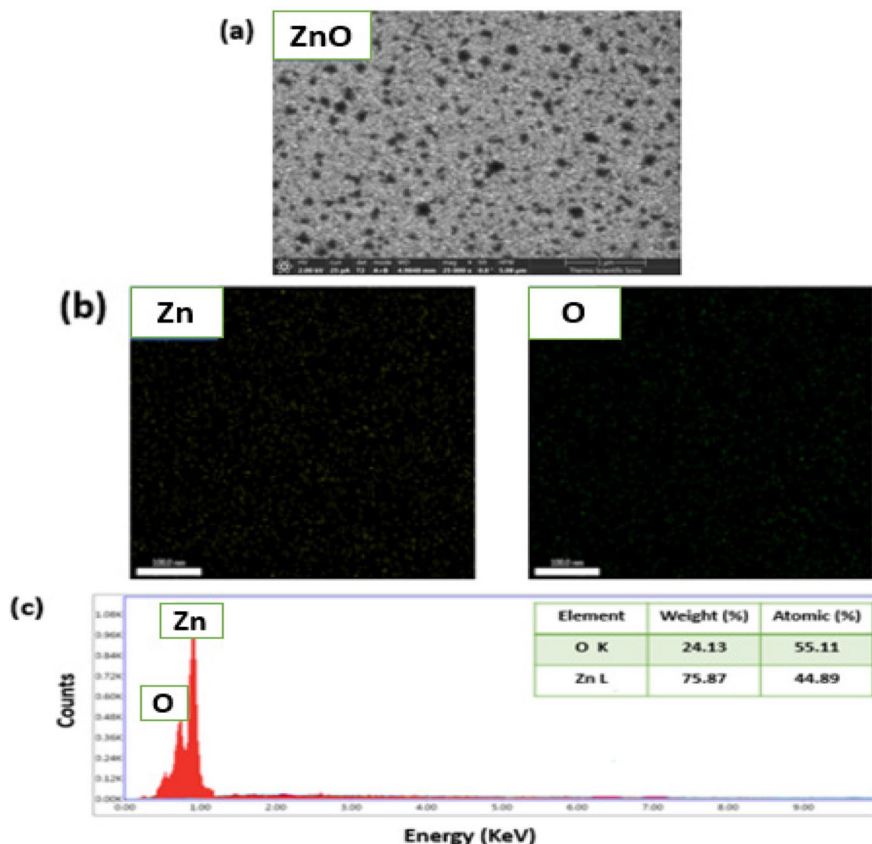


Fig. 3 XRD pattern of the ZnO (250 nm) thin film. The inset shows the ZnO (100) peak fitted for the grain size calculation

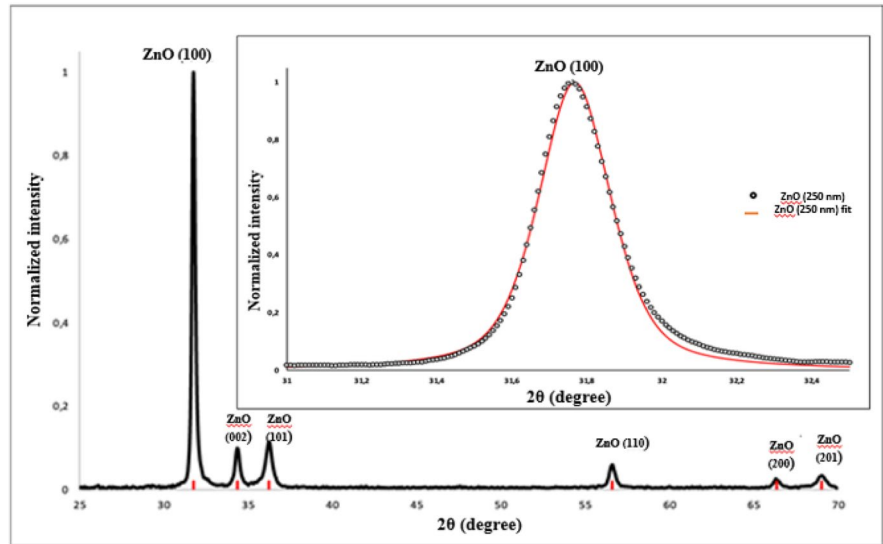


Table 1 Grain size calculations from ZnO (100) peak

Samples	2θ ⁰	Radian (θ ⁰)	Cos radian (θ ⁰)	β ⁰ (FWHM)	Radian β ⁰	Shape factor	D crystallite size (nm)
ZnO 250 nm	31.7667	15.88335	0.9618	0.23069	0.004026	0.89	35.41

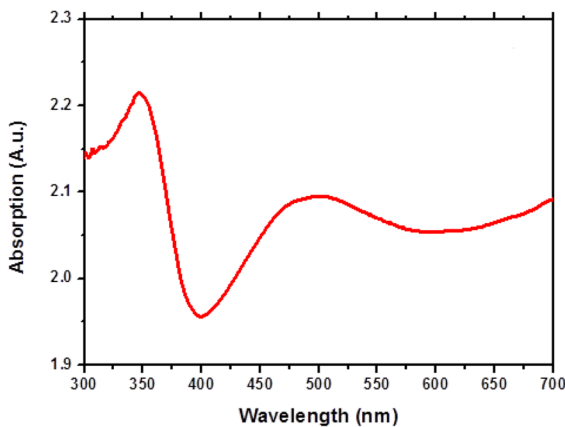


Fig. 4 Absorption spectra of the ZnO (250 nm) thin film

[20]. Table 1 presents the grain size calculations from the ZnO (100) peak.

UV-vis absorption and optical energy gap (E_g)

The optical absorption in the ultraviolet-visible (UV-vis) region depends on the structure of the sample. Figure 4 shows the significant absorption of the ZnO

thin film. The broad absorption band in the range (400–600 nm) was attributed to multiple vibration excitations [21].

The absorption coefficient α can be calculated from the absorbance according to the simple relation $\alpha = (2.303A)/t$, where A is the absorbance and t is the thickness of the film. Normally and according to the references, ZnO has a direct band gap, so the optical band gap E_g can be calculated with the following equation [21, 22]:

$$(\alpha h\nu)^2 = B(h\nu - E_g) \tag{1}$$

where $h\nu$ is the photon energy, B is a constant, and α is the absorption coefficient. The linear dependence of $(\alpha h\nu)^2$ on $h\nu$ is shown in Fig. 5

The estimated E_g is ≈ 3.32 eV with direct carrier transition. A review of the literature reveals that among various metal oxides, ZnO is one of the most important multifunctional crystalline wide band gaps due to its superior electronic and optical properties [22–24]. Good agreement was obtained when comparing the optical energy gap values of ZnO in the literature ($3.0 \text{ eV} < E_g < 3.4 \text{ eV}$), with the value estimated from the absorption

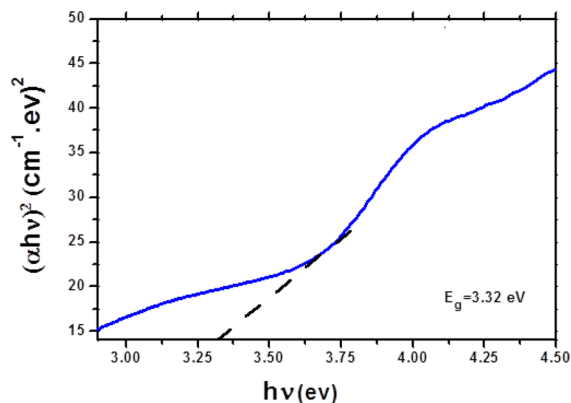


Fig. 5 Plot of $(\alpha h\nu)^2$ versus photon energy for the ZnO (250 nm) thin film

measurements [1, 2, 7, 19, 25]. The refractive index, or index of refraction, is defined as the quotient of the speed of light as it passes through two media. It is a dimensionless quantity that depends on the wavelength of the light beam; in other words, the refractive index is a measure of how light propagates through a material. The higher the refractive index, the slower the light travels, causing a correspondingly increased change of the direction of the light within the material. Different theories given in Eqs. 2 to 7 are used to calculate the refractive index $n_{(1)}$ to $n_{(6)}$, respectively, based on the value of the optical energy gap by:

Moss relation [26]

$$n_{(1)}^4 E_g = 95 \text{ eV} \quad (2)$$

Gupta et al. [27]

$$n_{(2)} = \frac{n^2 - 1}{n^2 + 2} = 1 - \sqrt{\frac{E_g}{20}} \quad (3)$$

Kumar and Singh relation [28]

$$n_{(3)} = K(E_g)^c \quad (4)$$

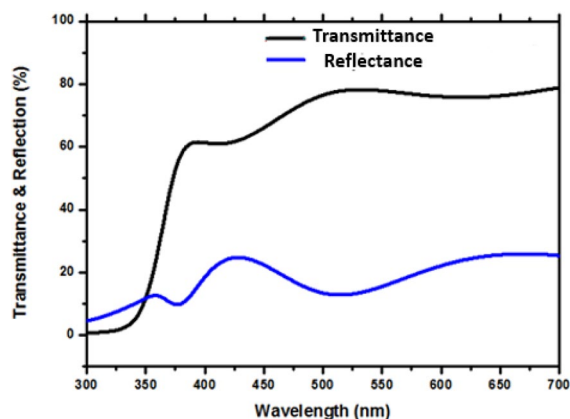


Fig. 6 Transmittance and reflection spectra of the ZnO (250nm) thin film

where $k = 3.3668$ and $c = -0.32234$.

Herve-Vandamme relation [29]

$$n_{(4)}^2 = 1 + \left[\frac{A}{E_g + B} \right]^2 \quad (5)$$

where $A = 13.6 \text{ eV}$ and $B = 3.47 \text{ eV}$.

Reddy relation [30]

$$n_{(5)}^4 [E_g - 0.365] = 154 \quad (6)$$

Ravindra relation [31]

$$n_{(6)} = 4.16 - 0.85 E_g \quad (7)$$

The refractive index values determined from the above equations are given in Table 2. This finding confirms that there is strong agreement between the refractive index values of $n_{(1)}$, $n_{(2)}$, $n_{(3)}$, and $n_{(4)}$, while the results for $n_{(5)}$ and $n_{(6)}$ given by the Reddy [30] and Ravindra [31] relations are completely ignored, as they are different from the others and can be neglected. The average values of the refractive index $n_{(av)}$ given by Eqs. 2, 3, 4, and 5 are summarized in Table 2.

Table 2 Values of the optical energy gap (E_g) and refractive index (n) for ZnO (250nm) thin films

Samples	Energy gap (E_g) (eV)	$n_{(1)}$	$n_{(2)}$	$n_{(3)}$	$n_{(4)}$	$n_{(5)}$	$n_{(6)}$	$n_{(av)}$
ZnO (250 nm)	3.32	2.31	2.31	2.28	2.26	2.68	1.338	2.29

Transmittance (T) and reflectance (R)

The optical transmittance (T) and reflectance (R) of the ZnO thin film in view of the incident wavelength are shown in Fig. 6. As seen, the ZnO thin film has high transmittance, and the average transmittance in the visible range around 80%.

The increase in transmittance and absorption may be related to the Moss-Burstein effect and the crystallinity of the film under study. Comparing Fig. 4 and Fig. 6, the inverse proportion of transmittance and absorption can be seen with the increase of the wavelength. The optical constants, the refractive index n , and the extinction coefficient k were determined using Murman’s equation [31] and a special iterative computer program, as previously discussed in [32, 33]. The variation of the dispersion parameters n and k with wavelength is shown in Fig. 7(a and b). The dispersion curve shows that the refractive index n first increases rapidly around the absorption edge and then decreases slowly with increasing wavelength, as shown in Fig. 7(a).

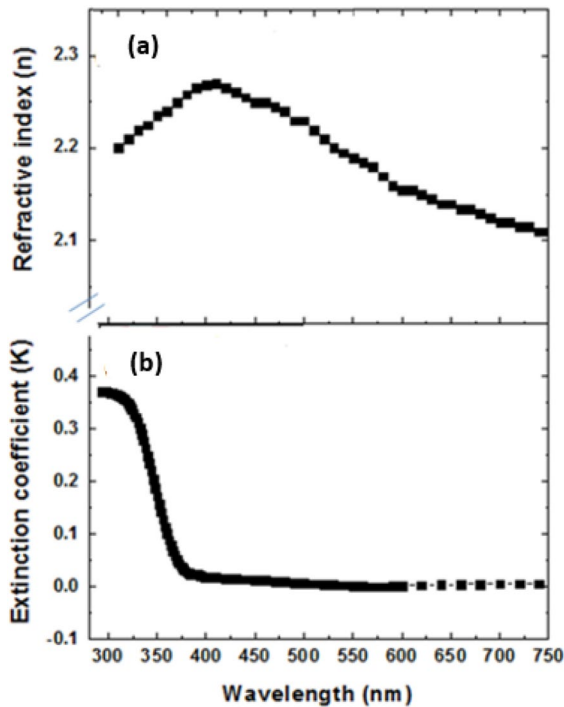


Fig. 7 Variation of the constants (a) n and (b) k versus the wavelength for the ZnO (250 nm) thin film

This behavior indicates a normal dispersion. The low calculated k values, including the total optical losses caused by both absorption and scattering in the visible region, Fig. 7(b), indicate the excellent transparency of our prepared ZnO thin film. The absorption coefficient (α) is related to k by the following relation $\alpha = (4\pi k/\lambda)$. Figure 8 shows the dependence of the absorption coefficient on the wavelength.

As seen in Fig. 8, the optical energy gap was graphically calculated using the intercept of the linear part of the curve $(\alpha h\nu)^2$ along $y = \text{zero}$. The estimated average band gap value is given in Table 3. The value of $E_g = 3.36$ eV estimated from the R and T measurements is higher than that estimated from the absorption measurements and is in excellent agreement with the value of E_g found in the literature [19]. The variability in the reported values of E_g can be rationalized based on the existence of a valence band-donor transition during preparation. To reveal the optical energy difference, the refractive index was calculated using the four proposed relations mentioned in Section 3.2. The calculated values are listed in Table 3. The average refractive index is equal to $n_{(av)} = 2.272$. The agreement between the average refractive index determined from the absorption measurements and that determined from the extinction coefficient is very good (99.56%). In general, for ZnO thin films with $3.07 \text{ eV} < E_g < 3.4 \text{ eV}$, the predicted refractive indices are valid for the four equations used for the ZnO thin film; neglecting Eqs. 6 and 7 as mentioned earlier in Section 3.2.

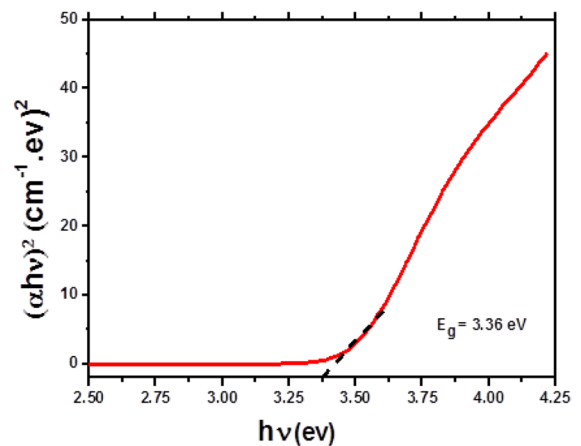


Fig. 8 Variation of $(\alpha h\nu)^2$ versus $(h\nu)$ for the ZnO (300 nm) thin film

Table 3 Direct optical energy gap (E_g) and refractive index (n) for ZnO thin films

Samples	Energy gap (E_g) (eV)	$n_{(1)}$	$n_{(2)}$	$n_{(3)}$	$n_{(4)}$	$n_{(5)}$	$n_{(6)}$	$n_{(av)}$
ZnO (250 nm)	3.36	2.30	2.30	2.27	2.24	2.686	1.304	2.277

Factors affecting the determination of the energy gap and the refractive index

The understanding of the optical energy gap (E_g) and refractive index (n) behavior is generally of prime importance, which has not been fully understood up to now. Therefore, in Table 4, we compare the optical energy gap and refractive index we obtained with some previously published results for samples prepared under conditions like the ZnO thin films we deposited.

It was found that the growth temperature influenced the optical energy gap values and therefore the growth temperature should be considered [7]. As mentioned in many theoretical calculations, the formation energy depends on ZnO-rich conditions, and a lower formation energy (100 °C) means a higher concentration of defects that affects the optical and electrical parameters of ZnO. At high growth temperatures, in the range of 200–300 °C, with Zn-rich conditions, the high concentration of oxygen vacancies creates an impurity level within the energy gap. The band gap energies are no longer related to the thickness of the layer. As mentioned in [1], the band gaps depend on the applied growth temperature, and the wide energy gap appears for a lower growth temperature than for a higher temperature.

Dielectric properties of ZnO thin film

The dielectric properties of ZnO define its characteristic role in electronics. It is considered a key element for various thin-film electronic systems because of its

superior dielectric and mechanical properties. The dielectric response of solid materials can be described in the form of a complex relative permittivity $\epsilon^*(\omega)$ by the equation [34]:

$$\epsilon^*(\omega) = \epsilon'(\omega) + j \epsilon''(\omega) \quad (8)$$

where $\epsilon' = \frac{C_p t}{\epsilon_o a}$ and $\epsilon'' = \epsilon' \tan \delta$ represent the real and imaginary parts of the dielectric permittivity, respectively, and C_p is the capacitance in parallel, ϵ_o is the free space permittivity, t is the thickness, and a is the cross sectional area of the sample. The frequency dependence of the dielectric constants ϵ' , ϵ'' , and $\tan \delta$ for ZnO film samples of thickness 300 nm in the frequency range of 1 kHz to 1 MHz and the temperature range of 303 to 413 K is presented in Fig. 9(a–c).

These variations of ϵ' and ϵ'' reveal that the value of ϵ' and ϵ'' increases with increasing temperature, while their behavior is inversely proportional to the applied field frequency. At a frequency above 8 kHz, the permittivity is weakly frequency and temperature dependent. This behavior can be assigned to the fact that at low frequencies, charge carriers respond faster to the externally applied electric field, resulting in higher values of the dielectric constants. At high frequencies, the charge carriers are unable to follow the rapid changes in the applied electric field, resulting in a decrease in the values of ϵ' and ϵ'' , as shown in Fig. 9(a and b) [35]. $\tan \delta$ quantifies the dissipation of electrical energy due to different physical processes. This quantity provides an alternative way to quantify the effect of loss on the electromagnetic field within a material. In our

Table 4 Optical parameters for the studied ZnO film and previously published data

ZnO prepared by ALD	As-grown temperature	Grain size (nm)	E_g (eV)	n
Our results	203 °C	35.41	3.32–3.36	2.27–2.29
Ref. [15]	200 °C	-	3.29	-
Ref. [1]	200 °C	-	3.274	2.1–2.9
Ref. [20]	350 °C	14.62	3.27	3.5
Ref. [13]	200 °C	-	3.37	-

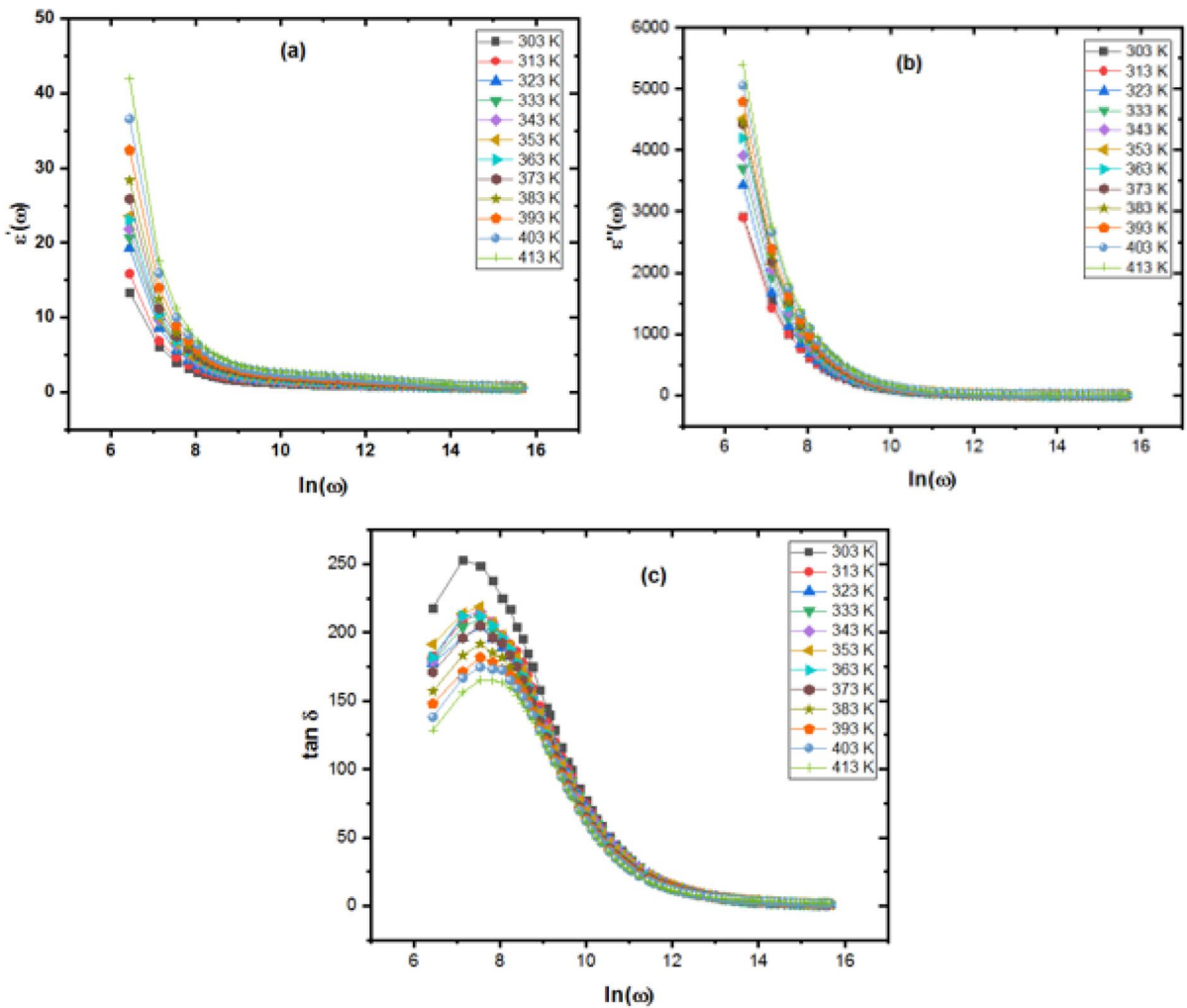


Fig. 9 Dielectric constants (a) ϵ' , (b) ϵ'' , and (c) $\tan \delta$ vs. frequency at various temperatures of ZnO (250 nm) thin film

results, a small shift in the peak of the loss tangent toward lower temperatures is observed when the frequency increases, as shown in Fig. 9(c). To explore the rate of increase of ϵ' and ϵ'' at various frequencies and temperatures, Fig. 10(a and b) presents the value of ϵ' and ϵ'' as a function of temperature. As noted, at low frequency, there is a non-linear increase in the ϵ' and ϵ'' values with increasing temperature, while at higher frequency, the behavior of ϵ' and ϵ'' are almost temperature independent. The observed behavior of both ϵ' and ϵ'' resembles that reported in previous articles [34, 36, 37].

The AC conductivity of ZnO thin films

The temperature dependence of the AC conductivity σ_{ac} was studied for ZnO thin films in the frequency range of 1 kHz to 1 MHz and in the temperature range of 303 to 413 K. The variation of $\ln \sigma_{ac}$ versus $1000/T$ for the ZnO thin film at different frequencies is shown in Fig. 11. As seen, the behavior of $\sigma_{ac}(\omega)$ increases with increasing temperature, suggesting that the AC conductivity is a thermally activated process with different localized states in the bandgap or its tail.

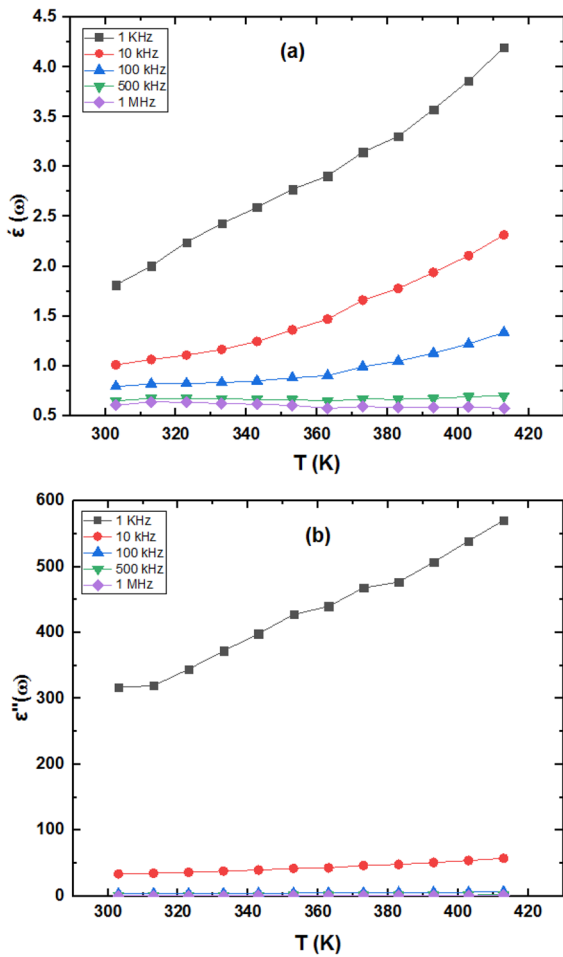


Fig. 10 Dependence of (a) ϵ' and (b) ϵ'' on temperature for the ZnO thin film (250 nm) at different frequencies

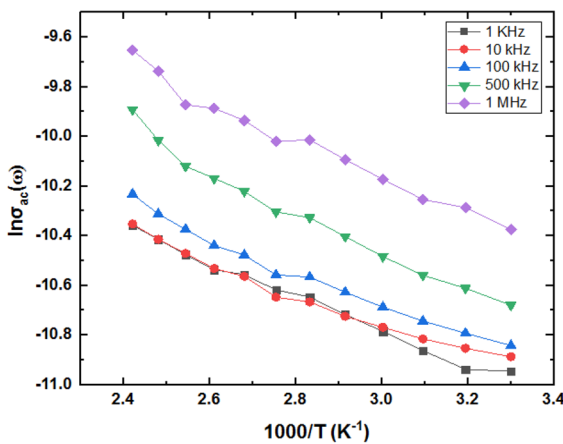


Fig. 11 AC conductivity of ZnO (250 nm) thin films versus reciprocal temperature

The activation energy ΔE_{σ} values for ZnO thin films at different frequencies were calculated using the following equation [38]:

$$\sigma_{ac}(\omega) = \sigma_o(\omega)\exp[\Delta E_{\sigma}(\omega)]/(k_B T) \tag{9}$$

where $\sigma_o(\omega)$ is the preexponential factor. The frequency dependence of $\Delta E_{\sigma}(\omega)$ is plotted in Fig. 12.

The graph shows that $\Delta E_{\sigma}(\omega)$ decreases with increasing frequency. This could be attributed to the applied frequency that improves the electronic jump between localized states [27, 38, 39]. The values of ΔE_{σ} agree with those obtained in the literature [27]. We have experimentally investigated that the higher conductivity is associated with lower activation energies and vice versa. Similarly, the higher the activation energy, the smaller the energy gap. Although there are explanations for this at phenomenological level, there is no consistent physical picture to explain the correlation between conductivity and activation energy [27, 39, 40]. In general, σ_{ac} increases with increasing frequency in the range of 100 Hz to 100 kHz, according to the Jonscher power law [40]:

$$\sigma_{ac}(\omega) = A\omega^s \tag{10}$$

where A is a constant, ω is the angular frequency, and s is the frequency exponent which varies ($0 < s \leq 1$) and depends on the temperature. The dependence of σ_{ac} on frequency within the investigated temperature range for the ZnO thin film is presented in Fig. 13.

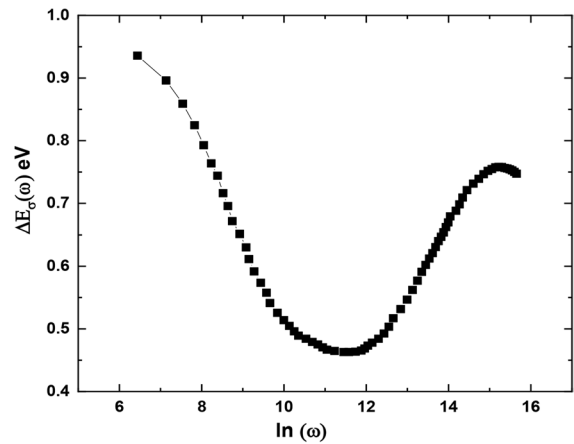


Fig. 12 AC activation energy vs. frequency for the ZnO thin film (250 nm)

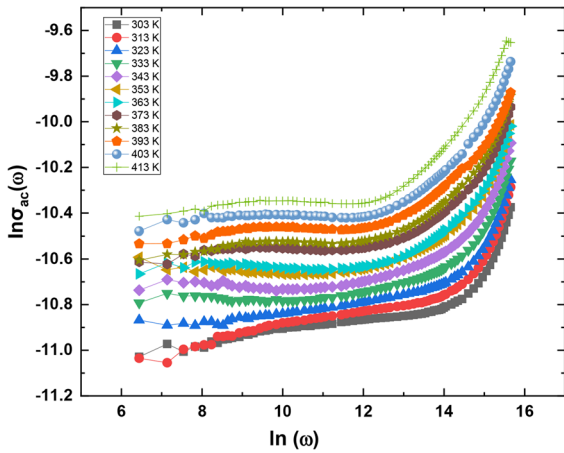


Fig. 13 Frequency dependence of AC conductivity for the ZnO (250 nm) thin film at different temperatures

As seen at low frequency, the conductivity is almost constant and is attributed to the long-range motion of charge carriers. As the frequency increases, the conductivity exhibits a strong frequency dependent resulting from the short-range hopping of the localized charge carriers at the grain boundaries as seen in Fig. 13. The study of the change of the frequency exponent s with the temperature makes it possible to determine the dominant conduction mechanism in semiconductor materials. The values of s can be obtained from the slopes of the linear lines seen in Fig. 13 in the frequency range of 1 kHz to 1 MHz. The average values of s are plotted as a function of temperature, as illustrated in Fig. 14(a).

It is obvious that the exponent values s is around 0.91 at room temperature, suggesting the correlated barrier hopping (CBH) model [37, 41–43]. In that situation, AC conductivity may be described by charge carrier hopping between pairs of localized states separated by a potential barrier. The power law dependence of σ_{ac} on frequency is due to short-range hopping of the charge carrier across trap sites separated by various heights of energy barriers and may be related to an increase in contact dipole charge carriers [41].

According to the correlated barrier hopping (CBH) model [44], (s) follows the formula:

$$s = - \frac{6 k_B T}{W_m + k_B T \ln(\omega \tau_o)} \tag{11}$$

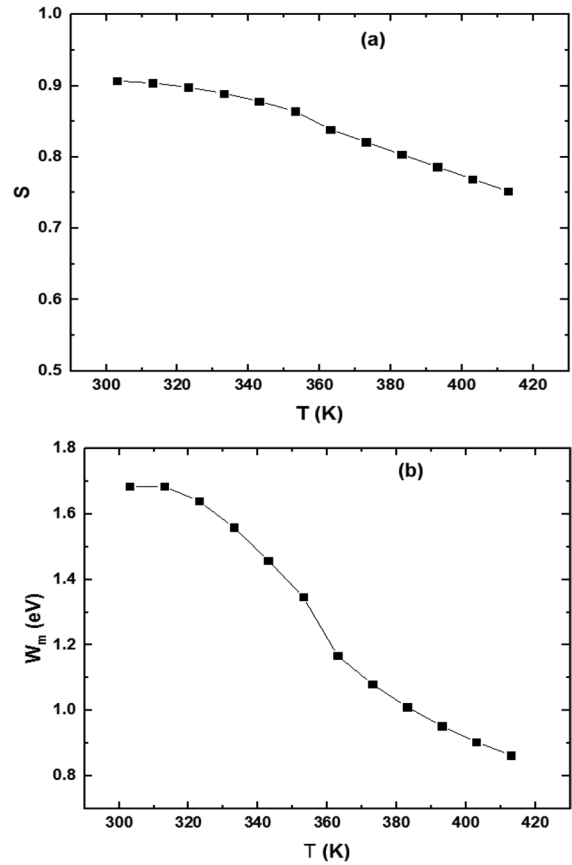


Fig. 14 Temperature dependence of (a) frequency exponent s and (b) W_m for the ZnO (250 nm) thin film

where k_B is Boltzmann’s constant, W_m is the maximum barrier height, and τ_o is the distinctive relaxation time, which is almost equal to the period of atomic vibration ($\tau_o = 10^{-12}$ s). The exponent (s) tends to be unity for large values of W_m ($W_m = KT$), so Eq. 11 can be simplified as follows [44]:

$$s = 1 - \frac{6 k_B T}{W_m} \tag{12}$$

Figure 14(b) represents the dependence of the calculated values of W_m on temperature and shows a gradual decrease with temperature. The obtained values of $W_m \ll E_g$ are in good agreement with Elliott’s theory of charge carrier hopping across the potential barrier in semiconductor materials and are close enough to the published data [45, 46].

Conclusions

In conclusion, we studied in detail the structural characterization, optical, and electrical analysis of ZnO thin films prepared by atomic layer deposition (ALD). In this study, we performed scanning electron microscopy (SEM), energy dispersive X-ray spectrometer (EDX), X-ray diffraction, absorption, transmittance, reflection, dielectric properties, and AC electrical conductivity measurements. The observed changes in the optical energy gap E_g and refractive index n values of the ZnO thin film were influenced by the deposition condition and the equations used to determine the parameters mentioned above. The frequency dependence of the dielectric constants ϵ' and ϵ'' has been investigated. AC conductivity σ_{ac} was analyzed using the universal power law and could be explained using the correlated barrier hopping (CBH) model. The optical, dielectric, and electrical properties of the ZnO thin film were used to make the decision on the appropriate model that can be proposed.

Acknowledgements The samples used in this study were prepared, and their morphology and uniformity were measured at the University of Debrecen, Hungary, according to the agreement between the Faculty of Education, Ain Shams University, "Coordinator and Supervisor Prof. Dr. Suzan Fouad" and the Faculty of Science and Technology, University of Debrecen, "Coordinator and Supervisor Prof. Dr. Zoltán Erdélyi." The optoelectrical parameters were measured at the central lab of physics department, Faculty of Education Ain Shams University. Project No. TKP2021-NKTA-34 has been implemented with the support provided from the National Research, Development and Innovation Fund of Hungary, financed under the TKP2021-NKTA funding scheme.

Author contribution S.S. Fouad: idea, writing revision, and data analysis. Eszter Baradács and Bence Parditka: sample preparation and XRD measurements. H.E. Atyia, A.M. Ismail, and M. Nabil: optical, SEM, AC conductivity measurements, and calculation parameters. Zoltán Erdélyi: preparation, writing, revision, XRD data analysis, spectroscopic ellipsometry measurements, and data analysis.

Data and code availability All data generated or analyzed during this study are included in this published article.

Compliance with ethical standards

Ethical approval Not applicable.

Conflict of interest The authors declare no competing interests.

References

- Zaka H, Parditka B, Erdélyi Z, Atyia HE, Sharma P, Fouad SS (2020) Investigation of dispersion parameters, dielectric properties and opto-electrical parameters of ZnO thin film grown by ALD. *Optik* 203:163933
- Shaba EY, Jacob JO, Tijani JO, Suleiman MAT (2021) A critical review of synthesis parameters affecting the properties of zinc oxide nanoparticle and its application in wastewater treatment. *Appl Water Sci* 11(2):1–41
- Bandeira M, Giovanela M, Roesch-Ely M, Devine DM, da Silva J, Crespo (2020) Green synthesis of zinc oxide nanoparticles: a review of the synthesis methodology and mechanism of formation. *Sustain Chem Pharm* 15:100223
- Ealia S, Anu Mary, Saravanakumar MP (2017) "A review on the classification, characterisation, synthesis of nanoparticles and their application." In IOP conference series: materials science and engineering, vol. 263, 3, p. 032019. IOP Publishing
- Ahmadipour M, Ain MF, Ahmad ZA (2016) Effect of thickness on surface morphology, optical and humidity sensing properties of RF magnetron sputtered CCTO thin films. *Appl Surf Sci* 385:182–190
- Ahmadipour M, Ayub SN, Ain MF, Ahmad ZA (2017) Structural, surface morphology and optical properties of sputter-coated $\text{CaCu}_3\text{Ti}_4\text{O}_{12}$ thin film: influence of RF magnetron sputtering power. *Mater Sci Semicond Process* 66:157–161
- Ahmadipour M, Ain MF, Ahmad ZA (2017) Effects of annealing temperature on the structural, morphology, optical properties and resistivity of sputtered CCTO thin film. *J Mater Sci Mater Electron* 28:12458–12466
- Ahmadipour M, Cheah WK, Ain MF, Rao KV, Ahmad ZA (2018) Effects of deposition temperatures and substrates on microstructure and optical properties of sputtered CCTO thin film. *Mater Lett* 210:4–7
- Ahmadipour M, Ain MF, Goutham S, Ahmad ZA (2018) Effects of deposition time on properties of $\text{CaCu}_3\text{Ti}_4\text{O}_{12}$ thin film deposited on ITO substrate by RF magnetron sputtering at ambient temperature. *Ceram Int* 44(15):18817–18820
- Mohammadihooyeh M, Karamian E, Emadi R (2019) The impact of MgAl_2O_4 nano-particles on the hydration-resistance improvement of dolomite-based refractories. *Ceram Int* 45(16):20674–20677
- Mohsen A, Arjmand M, Ain MF, Ahmad ZA, Pung S-Y (2019) Effect of Ar: N_2 flow rate on morphology, optical and electrical properties of CCTO thin films deposited by RF magnetron sputtering. *Ceram Int* 45(12):15077–15081
- Ahmadipour M, Ain MF, Ahmad ZA (2016) Fabrication of resistance type humidity sensor based on $\text{CaCu}_3\text{Ti}_4\text{O}_{12}$ thick film. *Measurement* 94:902–908
- Zhai C-H, Zhang R-J, Chen X, Zheng Y-X, Wang S-Y, Liu J, Dai N, Chen L-Y (2016) Effects of Al doping on the properties of ZnO thin films deposited by atomic layer deposition. *Nanoscale Res Lett* 11(1):1–8
- Raha S, Ahmaruzzaman M (2022) ZnO nanostructured materials and their potential applications: progress, challenges and perspectives. *Nanoscale Adv* 4(8):1868–1925
- Adhikari A, Przewdziecka E, Mishra S, Sybilski P, Sajkowski J, Guziejewicz E (2021) Optical properties of ZnO deposited by atomic layer deposition on sapphire: a comparison of thin and thick films. *Phys Status Solidi A* 218(17):2000669

16. Yadav SK, Atyia HE, Fouad SS, Sharma A, Mehta N (2023) Study of linear and non-linear optoelectronic properties of thermally grown thin films of amorphous selenium doped with graphene, multiwalled carbon nanotubes, and silver nanoparticles. *Diam Relat Mater* 136:110030
17. Fouad SS, Parditka B, Nabil M, Baradács E, Negm S, Atyia HE, Erdélyi Z (2021) Bilayer number driven changes in polarizability and optical property in ZnO/TiO₂ nanocomposite films prepared by ALD. *Optik* 233:166617
18. Jiang J, Pi J, Cai J (2018) The advancing of zinc oxide nanoparticles for biomedical applications. *Bioinorg Chem Appl* 2018:1–18
19. Kim JY, Liu G, Shim GY, Kim H, Lee JK (2020) Functionalized Zn@ ZnO hexagonal pyramid array for dendrite-free and ultrastable zinc metal anodes. *Adv Funct Mater* 30(36):2004210
20. Benhaliliba M (2021) ZnO a multifunctional material: physical properties, spectroscopic ellipsometry and surface examination. *Optik* 241:167197
21. El-Radaf IM, Al-Zahrán HYS, Fouad SS, El-Bana MS (2020) Profound optical analysis for novel amorphous Cu₂FeSnS₄ thin films as an absorber layer for thin film solar cells. *Ceram Int* 48(11):18778–18784
22. Nabil M, Mohamed SA, Easawi K, Obayya SSA, Negm S, Talaat H, El-Mansy MK (2020) Surface modification of CdSe nanocrystals: application to polymer solar cell. *Curr Appl Phys* 20(3):470–476
23. Fouad SS, Eszter Baradács M, Nabil BP, Negm S, Erdélyi Z (2022) Microstructural and optical duality of TiO₂/Cu/TiO₂ trilayer films grown by atomic layer deposition and DC magnetron sputtering. *Inorg Chem Commun* 145:110017
24. Nabil M, Easawi K, Abdallah T, Abdallah S, Elmancy MK, Negm S, Talaat H (2019) Performance enhancement of TBAI capped CdSe-quantum dot sensitized solar cells by an interlayer gold nanoparticles. *Am Acad Sci Res J Eng Technol Sci* 53(1):27–42
25. Fouad SS, Parditka B, Nabil M, Baradács E, Negm S, Erdélyi Z (2022) Effect of Cu interlayer on opto-electrical parameters of ZnO thin films. *J Mater Sci Mater Electron* 33:20594–20603
26. Fouad SS, Parditka B, Atyia HE, Baradács E, Erdélyi Z (2022) The real role of Cu metallic interlayer on the dielectric dispersion and conduction mechanism of TiO₂/Cu/TiO₂ nanolaminates. *Optik* 260:169078
27. Atyia HE, Fouad SS, Pal SK, Srivastava A, Mehta N (2022) Study of optical bandgap and other related optical properties in amorphous thin films of some optical materials of Se-Te-Sn-Ag system. *Opt Laser Technol* 150:107985
28. Fouad SS, Parditka B, Atyia HE, Baradács E, Bekheet AE, Erdélyi Z (2022) AC conductivity and dielectric parameters studies in multilayer TiO₂/ZnO thin films produced via ALD technique. *Chin J Phys* 77:73–80
29. Atyia HE, Fouad SS, Pal SK, Mehta N (2022) Peculiarities of resistive switching in thin films of glassy SeTeSnGe system. *Mater Sci Eng B* 276:115561
30. Fouad SS, Atyia HE, Bekheet AE, Kumar A, Mehta N (2021) Phenomenology of electrical switching behavior of SeTeSnCd thin films for memory applications. *J Non-Cryst Solids* 571:121025
31. Fouad SS, Parditka B, Bekheet AE, Atyia HE, Erdélyi Z (2021) ALD of TiO₂/ZnO multilayers towards the understanding of optical properties and polarizability. *Opt Laser Technol* 140:107035
32. El-Metwally EG, Assim EM, Fouad SS (2020) Optical characteristics and dispersion parameters of thermally evaporated Ge₅₀In₄Ga₁₃Se₃₃ chalcogenide thin films. *Opt Laser Technol* 131:106462
33. Zaka H, Fouad SS, Parditka B, Bekheet AE, Atyia HE, Medhat M, Erdélyi Z (2020) Enhancement of dispersion optical parameters of Al₂O₃/ZnO thin films fabricated by ALD. *Sol Energy* 205:79–87
34. Pal SK, Mehta N, Fouad SS, Atyia HE (2020) Dielectric behavior of amorphous thin films of Se–Te–Sn–Ge system. *Solid State Sci* 104:106289
35. Hegab NA, Atyia HE (2007) Dielectric studies of amorphous As₄Te₃₃Ge₁₀Si₁₂ films. *J Ovonic Res* 3(5):93–102
36. Atyia HE, Hegab NA, Affi MA, Ismail MI (2013) Influence of temperature and frequency on the AC conductivity and dielectric properties for Ge₁₅Se₆₀Bi₂₅ amorphous films. *J Alloys Compd* 574:345–353
37. Fouad SS, Soliman LI, Baradács E, Sayed ME, Parditka B, Osman NF, Nabil M, Zoltán Erdélyi (2023) Advances for enhancing the electrical properties and microhardness activity of ZnO/Cu/ZnO thin films prepared by ALD. *J Mater Sci pp* 1–11. <https://doi.org/10.1007/s10853-023-08411-9>
38. Atyia HE, Hegab NA (2016) Dielectric relaxation behavior and conduction mechanism of Te₄₆As₃₂Ge₁₀Si₁₂ films. *Optik* 127(15):6232–6242
39. Mehta N, Fouad SS, Baradacs E, Parditka B, Atyia HE, Pal SK, Erdelyi Z (2023) Multilayer stack structural designing of titania and zinc white using atomic layer deposition (ALD) technique and study of thermally governed dielectric dispersion and conduction under alternating electric fields. *J Mater Sci Mater Electron* 34(8):708
40. Fouad SS, Atyia HE (2016) Investigation of AC conductivity, dielectric and thermodynamics properties of Se Te Pb glassy system. *J Alloys Compd* 688:1206–1213
41. Elliott SR (1987) AC conduction in amorphous chalcogenide and pnictide semiconductors. *Adv Phys* 36(2):135–217
42. El-Barry AMA, Atyia HE (2005) Dielectric relaxation and AC conductivity of XS (X ¼ Cd, Zn) compounds. *Physica B* 368:1–7
43. Sharma A, Kumar A, Mehta N (2015) Determination of density of defect states in glassy Se₉₈M₂ (M= Ag, Cd and Sn) alloys using ac conductivity measurements. *Measurement* 75:69–75
44. Ganaie M, Zulfeqar M (2021) Dielectric investigation of In₄Se_{96-x}S_x semiconductor: relaxation and conduction mechanism. *Microelectron Reliab* 116:114018
45. Elliott SR (1978) Temperature dependence of a.c. conductivity of chalcogenide glasses. *Philos Mag B* 37:553
46. Afifi MA, Bekheet AE, Elwahhab EA, Atyia HE (2001) AC conductivity and dielectric properties of amorphous In₂Se₃ films. *Vacuum* 61(1):9–17

Publisher's note Springer Nature remains neutral with regard to jurisdictional claims in published maps and institutional affiliations.

Springer Nature or its licensor (e.g. a society or other partner) holds exclusive rights to this article under a publishing agreement with the author(s) or other rightsholder(s); author self-archiving of the accepted manuscript version of this article is solely governed by the terms of such publishing agreement and applicable law.